CP violation in B-$\bar{B}$ mixing with dilepton events

K. Abe,[10] K. Abe,[46] N. Abe,[49] I. Adachi,[10] H. Aihara,[48] M. Akatsu,[24] Y. Asano,[53]
T. Aso,[52] V. Aulchenko,[2] T. Aushev,[14] T. Aziz,[44] S. Bahinipati,[6] A. M. Bakich,[43]
Y. Ban,[36] M. Barbero,[9] A. Bay,[20] I. Bedny,[2] U. Bitenc,[15] I. Bizjak,[15] S. Blyth,[29]
A. Bondar,[2] A. Bozek,[30] M. Bračko,[22, 15] J. Brodzicka,[30] T. E. Browder,[9] M.-C. Chang,[29]
P. Chang,[29] Y. Chao,[29] A. Chen,[26] K.-F. Chen,[29] W. T. Chen,[26] B. G. Cheon,[4]
R. Chistov,[14] S.-K. Choi,[8] Y. Choi,[42] Y. K. Choi,[42] A. Chuvikov,[37] S. Cole,[43]
M. Danilov,[14] M. Dash,[55] L. Y. Dong,[12] R. Dowd,[23] J. Dragic,[23] A. Drutskoy,[6]
S. Eidelman,[2] Y. Enari,[24] D. Epifanov,[2] C. W. Everton,[23] F. Fang,[9] S. Fratina,[15]
H. Fujii,[10] N. Gabyshev,[2] A. Garmash,[37] T. Gershon,[10] A. Go,[26] G. Gokhroo,[44]
B. Golob,[21, 15] M. Grosse Perdekamp,[38] H. Guler,[9] J. Haba,[10] F. Handa,[47] K. Hara,[10]
T. Hara,[34] N. C. Hastings,[10] K. Hasuko,[38] K. Hayasaka,[24] H. Hayashii,[25] M. Hazumi,[10]
E. M. Heenan,[23] I. Higuchi,[47] T. Higuchi,[10] L. Hinz,[20] T. Hojo,[34] T. Hokuue,[24]
Y. Hoshi,[46] K. Hoshina,[51] S. Hou,[26] W.-S. Hou,[29] Y. B. Hsiung,[29] H.-C. Huang,[29]
T. Igaki,[24] Y. Igarashi,[10] T. Iijima,[24] A. Imoto,[25] K. Inami,[24] A. Ishikawa,[10] H. Ishino,[49]
K. Itoh,[48] R. Itoh,[10] M. Iwamoto,[3] M. Iwasaki,[48] Y. Iwasaki,[10] R. Kagan,[14] H. Kakuno,[48]
J. H. Kang,[56] J. S. Kang,[17] P. Kapusta,[30] S. U. Kataoka,[25] N. Katayama,[10] H. Kawai,[3]
H. Kawai,[48] Y. Kawakami,[24] N. Kawamura,[1] T. Kawasaki,[32] N. Kent,[9] H. R. Khan,[49]
A. Kibayashi,[49] H. Kichimi,[10] H. J. Kim,[19] H. O. Kim,[42] Hyunwoo Kim,[17] J. H. Kim,[42]
S. K. Kim,[41] T. H. Kim,[56] K. Kinoshita,[6] P. Koppenburg,[10] S. Korpar,[22, 15] P. Križan,[21, 15]
P. Krokovny,[2] R. Kulasiri,[6] C. C. Kuo,[26] H. Kurashiro,[49] E. Kurihara,[3] A. Kusaka,[48]
A. Kuzmin,[2] Y.-J. Kwon,[56] J. S. Lange,[7] G. Leder,[13] S. E. Lee,[41] S. H. Lee,[41]
Y.-J. Lee,[29] T. Lesiak,[30] J. Li,[40] A. Limosani,[23] S.-W. Lin,[29] D. Liventsev,[14]
J. MacNaughton,[13] G. Majumder,[44] F. Mandl,[13] D. Marlow,[37] T. Matsuishi,[24]
H. Matsumoto,[32] S. Matsumoto,[5] T. Matsumoto,[50] A. Matyja,[30] Y. Mikami,[47]
W. Mitaroff,[13] K. Miyabayashi,[25] Y. Miyabayashi,[24] H. Miyake,[34] H. Miyata,[32] R. Mizuk,[14]
D. Mohapatra,[55] G. R. Moloney,[23] G. F. Moorhead,[23] T. Mori,[49] A. Murakami,[39]
T. Nagamine,[47] Y. Nagasaka,[11] T. Nakadaira,[48] I. Nakamura,[10] E. Nakano,[33] M. Nakao,[10]
H. Nakazawa,[10] Z. Natkaniec,[30] K. Neichi,[46] S. Nishida,[10] O. Nitoh,[51] S. Noguchi,[25]
T. Nozaki,[10] A. Ogawa,[38] S. Ogawa,[45] T. Ohshima,[24] T. Okabe,[24] S. Okuno,[16]
S. L. Olsen,[9] Y. Onuki,[32] W. Ostrowicz,[30] H. Ozaki,[10] P. Pakhlov,[14] H. Palka,[30]
C. W. Park,[42] H. Park,[19] K. S. Park,[42] N. Parslow,[43] L. S. Peak,[43] M. Pernicka,[13]
J.-P. Perroud,[20] M. Peters,[9] L. E. Piilonen,[55] A. Poluektov,[2] F. J. Ronga,[10] N. Root,[2]
M. Rozanska,[30] H. Sagawa,[10] M. Saigo,[47] S. Saitoh,[10] Y. Sakai,[10] H. Sakamoto,[18]
T. R. Sarangi,[10] M. Satapathy,[54] N. Sato,[24] O. Schneider,[20] J. Schümann,[29] C. Schwanda,[13]
A. J. Schwartz,[6] T. Seki,[50] S. Semenov,[14] K. Senyo,[24] Y. Settai,[5] R. Seuster,[9]
M. E. Sevior,[23] T. Shibata,[32] H. Shibuya,[45] B. Shwartz,[2] V. Sidorov,[2] V. Siegle,[38]
J. B. Singh,[35] A. Somov,[6] N. Soni,[35] R. Stamen,[10] S. Stanič,[53, *] M. Starič,[15] A. Sugi,[24]
A. Sugiyama,[39] K. Sumisawa,[34] T. Sumiyoshi,[50] S. Suzuki,[39] S. Y. Suzuki,[10] O. Tajima,[10]
F. Takasaki,[10] K. Tamai,[10] N. Tamura,[32] K. Tanabe,[48] M. Tanaka,[10] G. N. Taylor,[23]
Y. Teramoto,[33] X. C. Tian,[36] S. Tokuda,[24] S. N. Tovey,[23] K. Trabelsi,[9] T. Tsuboyama,[10]

arXiv:hep-ex/0409012v1 2 Sep 2004

T. Tsukamoto,[10] K. Uchida,[9] S. Uehara,[10] T. Uglov,[14] K. Ueno,[29] Y. Unno,[3] S. Uno,[10]
Y. Ushiroda,[10] G. Varner,[9] K. E. Varvell,[43] S. Villa,[20] C. C. Wang,[29] C. H. Wang,[28]
J. G. Wang,[55] M.-Z. Wang,[29] M. Watanabe,[32] Y. Watanabe,[49] L. Widhalm,[13]
Q. L. Xie,[12] B. D. Yabsley,[55] A. Yamaguchi,[47] H. Yamamoto,[47] S. Yamamoto,[50]
T. Yamanaka,[34] Y. Yamashita,[31] M. Yamauchi,[10] Heyoung Yang,[41] P. Yeh,[29] J. Ying,[36]
K. Yoshida,[24] Y. Yuan,[12] Y. Yusa,[47] H. Yuta,[1] S. L. Zang,[12] C. C. Zhang,[12] J. Zhang,[10]
L. M. Zhang,[40] Z. P. Zhang,[40] V. Zhilich,[2] T. Ziegler,[37] D. Žontar,[21, 15] and D. Zürcher[20]

(The Belle Collaboration)

[1]Aomori University, Aomori
[2]Budker Institute of Nuclear Physics, Novosibirsk
[3]Chiba University, Chiba
[4]Chonnam National University, Kwangju
[5]Chuo University, Tokyo
[6]University of Cincinnati, Cincinnati, Ohio 45221
[7]University of Frankfurt, Frankfurt
[8]Gyeongsang National University, Chinju
[9]University of Hawaii, Honolulu, Hawaii 96822
[10]High Energy Accelerator Research Organization (KEK), Tsukuba
[11]Hiroshima Institute of Technology, Hiroshima
[12]Institute of High Energy Physics,
Chinese Academy of Sciences, Beijing
[13]Institute of High Energy Physics, Vienna
[14]Institute for Theoretical and Experimental Physics, Moscow
[15]J. Stefan Institute, Ljubljana
[16]Kanagawa University, Yokohama
[17]Korea University, Seoul
[18]Kyoto University, Kyoto
[19]Kyungpook National University, Taegu
[20]Swiss Federal Institute of Technology of Lausanne, EPFL, Lausanne
[21]University of Ljubljana, Ljubljana
[22]University of Maribor, Maribor
[23]University of Melbourne, Victoria
[24]Nagoya University, Nagoya
[25]Nara Women's University, Nara
[26]National Central University, Chung-li
[27]National Kaohsiung Normal University, Kaohsiung
[28]National United University, Miao Li
[29]Department of Physics, National Taiwan University, Taipei
[30]H. Niewodniczanski Institute of Nuclear Physics, Krakow
[31]Nihon Dental College, Niigata
[32]Niigata University, Niigata
[33]Osaka City University, Osaka
[34]Osaka University, Osaka
[35]Panjab University, Chandigarh
[36]Peking University, Beijing
[37]Princeton University, Princeton, New Jersey 08545

^{38}*RIKEN BNL Research Center, Upton, New York 11973*
^{39}*Saga University, Saga*
^{40}*University of Science and Technology of China, Hefei*
^{41}*Seoul National University, Seoul*
^{42}*Sungkyunkwan University, Suwon*
^{43}*University of Sydney, Sydney NSW*
^{44}*Tata Institute of Fundamental Research, Bombay*
^{45}*Toho University, Funabashi*
^{46}*Tohoku Gakuin University, Tagajo*
^{47}*Tohoku University, Sendai*
^{48}*Department of Physics, University of Tokyo, Tokyo*
^{49}*Tokyo Institute of Technology, Tokyo*
^{50}*Tokyo Metropolitan University, Tokyo*
^{51}*Tokyo University of Agriculture and Technology, Tokyo*
^{52}*Toyama National College of Maritime Technology, Toyama*
^{53}*University of Tsukuba, Tsukuba*
^{54}*Utkal University, Bhubaneswer*
^{55}*Virginia Polytechnic Institute and State University, Blacksburg, Virginia 24061*
^{56}*Yonsei University, Seoul*
(Dated: February 7, 2008)

Abstract

We report a measurement of the charge asymmetry for same-sign dileptons in B^0-$\bar{B}^0$ mixing. The data were collected with the Belle detector at KEKB. Using a data sample of 78 fb^{-1} recorded at the $\Upsilon(4S)$ resonance and 9 fb^{-1} recorded at an energy 60 MeV below the resonance, we measure $A_{sl} = (-0.13 \pm 0.60(\text{stat}) \pm 0.56(\text{sys}))\%$.

---

*on leave from Nova Gorica Polytechnic, Nova Gorica

I. INTRODUCTION

The standard model allows CP-violation in B^0-$\bar{B}^0$ mixing [1]. In particular, there is a possible difference between the $B^0 \to \bar{B}^0$ and $\bar{B}^0 \to B^0$ transition rates, which can manifest itself as a charge asymmetry in the same-sign dilepton events in $\Upsilon(4S)$ decays when prompt leptons from semileptonic decays of neutral B mesons are selected. With the assumption of CPT invariance in the mixing, the flavor and mass eigenstates of the neutral B mesons are related by

$$
\begin{aligned}
|B_H\rangle &= p|B^0\rangle + q|\bar{B}^0\rangle, \\
|B_L\rangle &= p|B^0\rangle - q|\bar{B}^0\rangle.
\end{aligned}
\tag{1}
$$

The time-dependent decay rate for same-sign dileptons is given by

$$
\Gamma_{\Upsilon(4S)\to\ell^+\ell^+}(\Delta t) = \frac{|A_l|^4}{8\tau_{B^0}} e^{-|\Delta t|/\tau_{B^0}} \left|\frac{p}{q}\right|^2 \left[\cosh\left(\frac{\Delta\Gamma}{2}\Delta t\right) - \cos\left(\Delta m_d \Delta t\right)\right]
\tag{2}
$$

for the $\ell^+\ell^+$ sample. For the $\ell^-\ell^-$ sample, p/q is replaced by q/p. Here Δm_d and $\Delta\Gamma$ are the differences in mass and decay width between the two mass eigenstates, τ_{B^0} is the average lifetime of the two mass eigenstates, Δt is the proper time difference between the two B meson decays. In this analysis only the absolute value of Δt is used. It is assumed that the semileptonic decay of the neutral B meson is flavour specific and CP conserving, so that $A_l = \bar{A}_l$. If CP is not conserved in mixing, the condition $|p/q| = 1$ is no longer required and the decay rates for $\ell^+\ell^+$ and $\ell^-\ell^-$ samples can differ. As can be seen in Eq. 2, the Δt dependence is the same for the $\ell^+\ell^+$ and $\ell^-\ell^-$ samples, and therefore the CP-violation shows up as a Δt-independent charge asymmetry, defined as

$$
A_{sl} \equiv \frac{\Gamma_{\Upsilon(4S)\to\ell^+\ell^+} - \Gamma_{\Upsilon(4S)\to\ell^-\ell^-}}{\Gamma_{\Upsilon(4S)\to\ell^+\ell^+} + \Gamma_{\Upsilon(4S)\to\ell^-\ell^-}} = \frac{1 - |q/p|^4}{1 + |q/p|^4} \simeq \frac{4Re(\epsilon_B)}{1 + |\epsilon_B|^2}.
\tag{3}
$$

Here ϵ_B corresponds to the ϵ_K describing CP-violation in the neutral K meson system. Standard Model calculations give the size of this asymmetry to be of the order of 10^{-3} [2, 3]. A significantly larger value would therefore be an indication of new physics.

Experimentally, measurement of same-sign dilepton events that originate from B^0B^0 and $\bar{B}^0\bar{B}^0$ initial states requires careful charge-dependent corrections, which must be done in several steps. First, the contribution from continuum $e^+e^- \to q\bar{q}$ (where $q = u, d, s$ or c) to same-sign dilepton events must be subtracted using off-resonance data. Second, all detected lepton tracks must be corrected for charge asymmetries in the efficiencies for track finding and lepton identification, and for the probabilities of misidentifying hadrons as leptons. After these corrections, the remaining same-sign dilepton events still contain backgrounds from $B^0\bar{B}^0$ and B^+B^- events. The last step of this analysis is to separate the signal events from these background events using their different behavior in the Δt distributions.

II. BELLE DETECTOR

The data were collected with the Belle detector [4] at the KEKB asymmetric e^+e^- collider [5].

The Belle detector is a large-solid-angle magnetic spectrometer that consists of a three-layer silicon vertex detector (SVD), a 50-layer central drift chamber (CDC) for tracking, a mosaic of aerogel threshold Cherenkov counters, time-of-flight scintillation counters (TOF), and an array of CsI(Tℓ) crystals for electromagnetic calorimetry (ECL) located inside of a superconducting solenoid coil that provides a 1.5 T magnetic field. An iron flux-return located outside of the coil is instrumented to detect K_L mesons and to identify muons (KLM). The integrated luminosity of the data sample is 78 fb^{-1} at the $\Upsilon(4S)$ resonance ("on-resonance") and 9 fb^{-1} at 60 MeV below from the $\Upsilon(4S)$ resonance ("off-resonance").

A. Track finding Efficiency

The track finding efficiency is determined by analyzing a sample where simulated single electron or muon tracks are overlaid on hadronic events taken from experimental data. Lepton tracks are generated to cover the region of 1.2 GeV/c < p^* < 2.3 GeV/c and 30° < θ_{lab} < 135°, where p^* is the lepton momentum in the e^+e^- center-of-mass (c.m.) and θ_{lab} is the angle of lepton track with respect to the z-axis in the laboratory frame. The z-axis passes through the nominal interaction point, and is anti-parallel to the positron beam direction. Figure 1 shows track finding efficiencies for positive and negative tracks separately and their fractional differences as a function of p^* for electron and muon tracks. Events in all $\theta_{\text{lab.}}$ regions are combined in these plots. The charge dependence of the track finding efficiency for both electrons and muons is less than 1.0%.

B. Lepton Identification

The most important contribution to the electron identification comes from examination of the ratio of the ECL cluster energy to the track momentum measured in the CDC. This information is combined with the shower measurement in the ECL, the specific ionization measurements (dE/dx) in the CDC, and the ACC light yield, to form an electron likelihood $\mathcal{L}_e$. [6]

The two-photon process $e^+e^- \to (e^+e^-)e^+e^-$ is used to estimate the electron identification efficiency. For this data sample, events are required to have: i) two tracks with particle ID information inconsistent with a muon hypothesis, laboratory momenta greater than 0.5 GeV/c and transverse momenta greater than 0.25 GeV/c; ii) at least one ECL cluster with energy greater than 20 MeV. The two tracks are required to have: i) an acolinearity angle whose cosine is greater than -0.997; ii) a transverse-momentum sum less than 0.2 GeV/c; and a longitudinal momentum sum of less than 2.5 GeV/c in the c.m. frame; iii) an invariant mass less than 5 GeV/c^2. In addition the sum of the ECL cluster energies must be between 0.6 GeV/c and 6.0 GeV/c. The electron identification efficiency is obtained by taking the ratio of the number of tracks selected with the above requirements with and without additional electron identification requirements.

For muon identification, CDC tracks are extrapolated to the KLM and the measured range and transverse deviation in the KLM is compared with the expected values to form a muon likelihood $\mathcal{L}_\mu$ [7].

The muon identification efficiency is determined by analyzing a data sample where simulated single-muon tracks are overlaid on the hadronic events taken from experimental data.

Figure 2 shows the charge-dependent lepton identification efficiencies, where electron

FIG. 1: Track finding efficiencies as a function of c.m. momentum for positron tracks ε_+ (a), electron tracks ε_- (b), and charge dependence defined as $(\varepsilon_+ - \varepsilon_-)/(\varepsilon_+ + \varepsilon_-)$. Corresponding plots for muon tracks are shown in (d), (e), and (f)

.

tracks are required to satisfy $\mathcal{L}_e > 0.8$ and the muon tracks are required to satisfy $\mathcal{L}_\mu > 0.9$ and the reduced χ^2, of the transverse deviation in the KLM is required to be less than 3.5. The charge dependence of both electron and muon identification efficiencies are less than 1%.

C. Hadron identification

Comparison of the ACC light yield to the track momentum, the time of flight measurement, and dE/dx measurements in the CDC are combined to provide hadron likelihoods, $\mathcal{L}_\pi$ for pions, $\mathcal{L}_K$ for kaons, and $\mathcal{L}_p$ for protons.
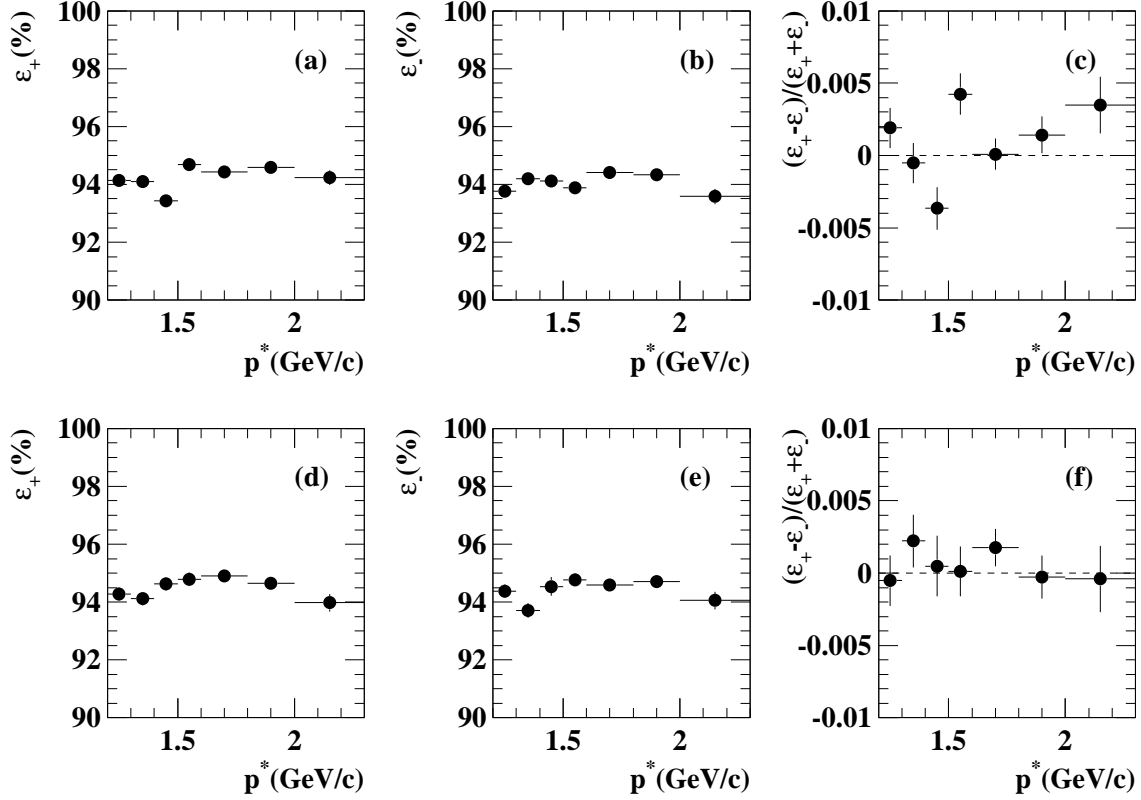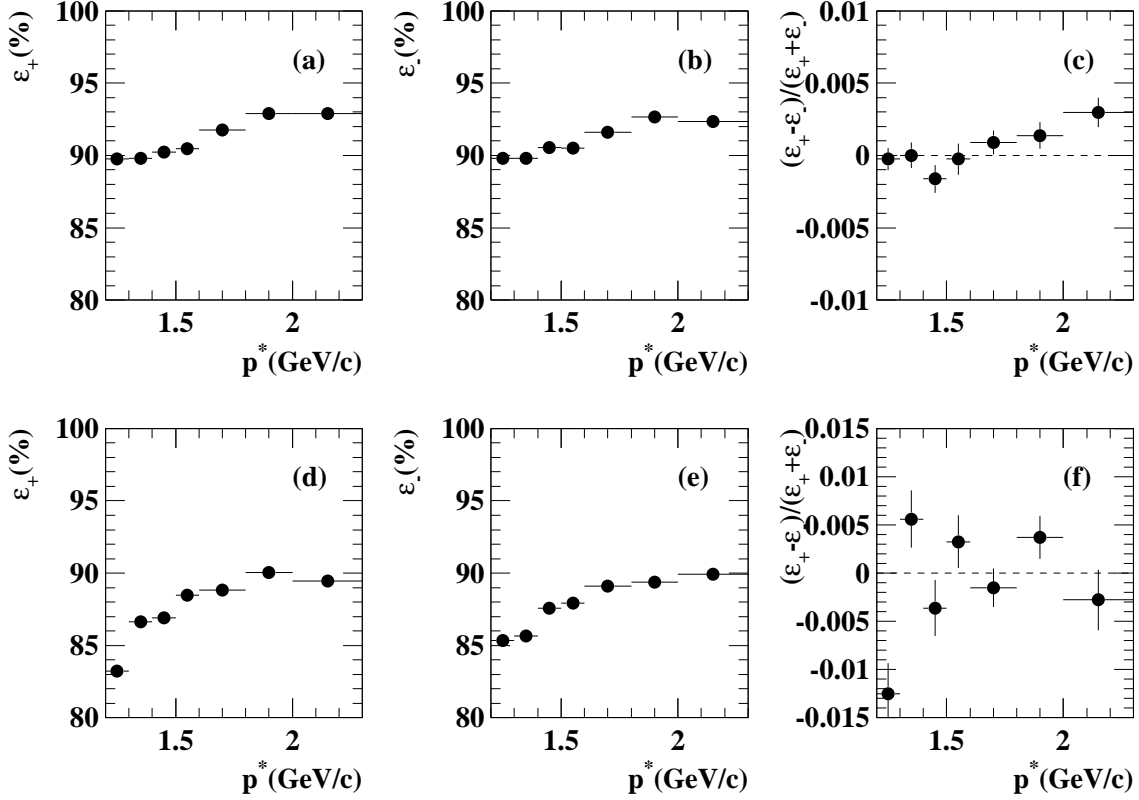
FIG. 2: Identification efficiencies as a function of c.m. momentum for positrons ε_+ (a), electrons ε_- (b), and charge dependence defined as $(\varepsilon_+ - \varepsilon_-)/(\varepsilon_+ + \varepsilon_-)$(c). Corresponding plots for muons are shown in (d), (e), and (f).

D. Fake lepton

The hadron fake rate, which is defined as the probability that a hadron track is mis-identified as a lepton, is determined from a sample of $K_s \to \pi^+\pi^-$ for pions, $\phi \to K^+K^-$ for kaons, and $\Lambda \to p\pi^-$ ($\bar{\Lambda} \to \bar{p}\pi^+$) for protons. These decays are selected from a hadronic event sample, which will be described later. To select these track pair combinations, the closest approach with respect to the run-dependent interaction point and the position of decay vertex are used. The z position distance of two tracks and the deflection angle (except for $\phi \to KK$) at the decay vertex are also used. For each decay, the invariant mass of the two tracks is calculated after imposing the hadron identification requirement on the negative (positive) charged track. The signal yields are obtained by fitting the resulting mass distributions to sums of double Gaussian signal terms and smooth background functions in two ways: once without imposing any particle identification requirement and again after imposing the lepton identification requirement on the positive (negative) charged track. The ratios of the two signal yields give the fake rates for the positive (negative) charged tracks. The following cuts are placed on the likelihood ratios: $\mathcal{L}_\pi/(\mathcal{L}_\pi + \mathcal{L}_K) > 0.8$ for pions

in $K_S \to \pi^+\pi^-$, $\mathcal{L}_K/(\mathcal{L}_K + \mathcal{L}_\pi) > 0.8$ for kaons in $\phi \to K^+K^-$, and $\mathcal{L}_\pi/(\mathcal{L}_\pi + \mathcal{L}_p) > 0.8$ for pions in $\Lambda \to p\pi^-$. The rate of pions faking electrons is at most 0.1% for both charges and shows no significant charge dependence. The rate of kaons faking electrons decreases rapidly as p_{lab} becomes larger and is less than 0.2% for $p_{\text{lab}} > 1.4$ GeV/c with no significant charge dependence. While the rate of protons faking electrons is nearly zero, the rate for anti-protons faking electrons is as large as 4% due to the large anti-proton annihilation cross section in the ECL. The rate of pions faking muons is about 1% for $p_{\text{lab}} > 1.5$ GeV/c and shows no significant charge dependence. The rate of kaons faking muons is 1% to 2% and that for K^+ is about 50% larger than K^- due to the larger kaon-nucleon cross section for the K^-. The rate of protons faking muons is less than 0.4% and shows no clear charge dependence.
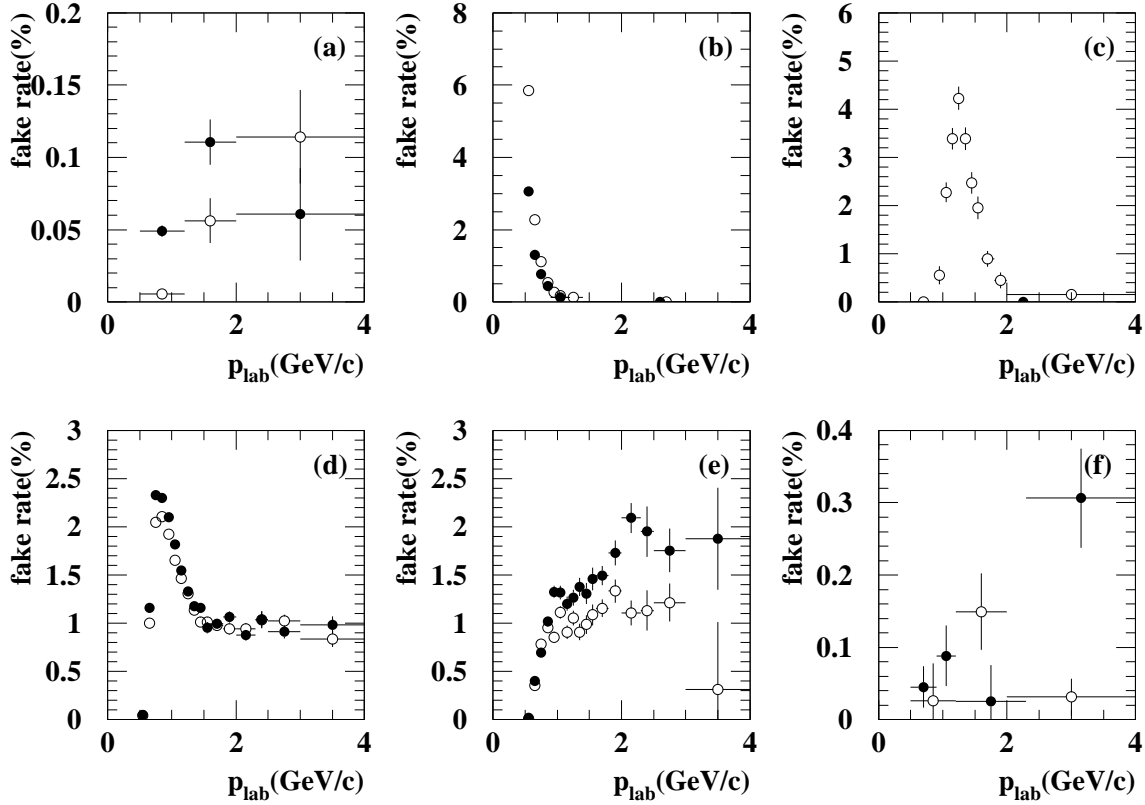

FIG. 3: Rates of pions ((a) and (d)), kaons ((b) and (e)), and protons ((c) and (f)) faking electrons and muons vs laboratory momentum. Filled circles are for positive tracks and open circles are for negative tracks. The increase in the rate of kaons faking electrons at low momentum clearly visible in (b) is due to the overlap of the electron and kaon energy loss bands.

III. EVENT SELECTION

A. Hadronic Event Selection

Hadronic events are required to have at least five tracks, an event vertex with radial and z coordinates within 1.5 cm and 3.5 cm respectively of the nominal beam interaction point, a total reconstructed c.m. energy greater than 0.5 W (W is the $\Upsilon(4S)$ c.m. energy), a net reconstructed c.m. momentum with a z component less than 0.3 W/c, a total energy deposited to ECL between 0.025 and 0.9 W, and a ratio R_2 of the second and zeroth Fox-Wolfram moments [8] less than 0.7.

B. Dilepton Event Selection

Lepton candidates are selected from the charged tracks by requiring $\mathcal{L}_e > 0.8$ for electrons or $\mathcal{L}_\mu > 0.9$ and a reduced χ^2 of the transverse deviation in the KLM of less than 3.5 for muons. In both cases a distance of closest approach to the run-dependent interaction point less than 0.05 cm radially and 2.0 cm in z is required. At least one SVD hit per track in the r-ϕ view and two SVD hits in the r-z view is required. To eliminate electrons from $\gamma \to e^+e^-$ conversions, electron candidates are paired with all other oppositely charged tracks and the invariant mass (assuming the electron mass hypothesis) $M_{e^+e^-}$ is calculated. If $M_{e^+e^-} < 100$ MeV/c^2, the electron candidate is rejected. If a hadronic event contains more than two lepton candidates, the two with the highest c.m. momenta are used.

The two lepton candidates must satisfy additional criteria. The c.m. momentum of each lepton is required to be in the range 1.2 GeV/$c < p^* < 2.3$ GeV/c. The lower cut reduces contributions from secondary charm decay. The upper cut reduces continuum contributions. Each lepton track must satisfy $30° < \theta_{\text{lab}} < 135°$. This cut selects tracks with better z vertex resolution and better lepton identification. Events that contain one or more J/ψ candidates are rejected. The invariant mass of each candidate lepton paired with each oppositely charged track (assuming the correct lepton mass hypothesis) is calculated. If the invariant mass falls into the J/ψ region, defined as -0.15 GeV/$c^2 < (M_{e^+e^-} - M_{J/\psi}) < 0.05$ GeV/c^2 or -0.05 GeV/$c^2 < (M_{\mu^+\mu^-} - M_{J/\psi}) < 0.05$ GeV/c^2, the candidate event is rejected. The looser lower cut for the electron pair invariant mass is used to reject J/ψ decays with a low invariant mass due to bremsstrahlung of the daughter electron(s).

As can be seen in Fig. 4, distributions of the opening angle of the two tracks in the c.m. frame, $\cos\theta^*_{\ell\ell}$, for the $\mu\mu$ and $e\mu$ pairs show distinct peaks in the back-to-back direction ($\cos\theta^*_{\ell\ell} \simeq -1$). This background is caused by jet-like continuum events and events with a primary lepton and a secondary lepton originating from the same B meson. Also spikes can be seen at $\cos\theta^*_{\ell\ell} = 1$ in the $\mu\mu$ pairs. This structure is caused by jet-like continuum events where a non-muon track is identified as muon because it is assigned hits in the KLM from a true muon. The opening dilepton angle in the c.m. frame $\theta^*_{\ell\ell}$ is required to satisfy $-0.80 < \cos\theta^*_{\ell\ell} < 0.95$ in order to reduce this background.

With these selection criteria there are 46551 positive and 45507 negative same sign dilepton events found in the on-resonance data. Continuum contributions are estimated to be 2229.8 for positive and 1556.5 for negative same sign events, based on the yield from off-resonance data. To estimate the continuum contribution from off-resonance data, off-resonance yields were scaled by the integrated luminosities and cross-section ratio. The scaling factor is defined in the Eq. 5. These dilepton yields decomposed into different lepton
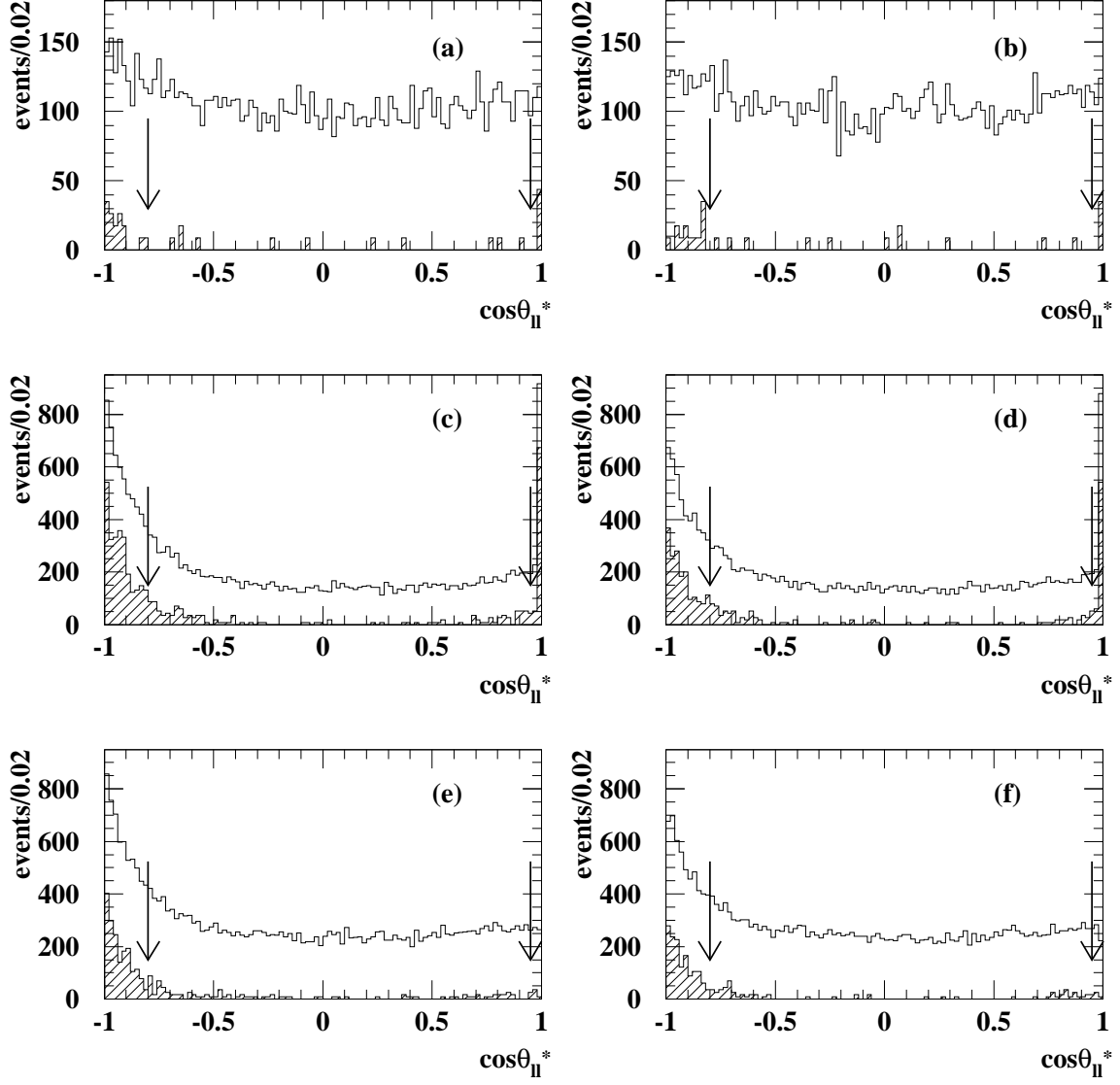
9

FIG. 4: $\cos\theta_{\ell\ell}^{*}$ distributions for the dilepton samples of the on-resonance (open histogram) and scaled off-resonance (filled histogram) data. (a),(b) show *ee* events, (c),(d) show $\mu\mu$ events and (e),(f) are from $e\mu$ combinations. (a),(c) and (e) are the $++$ charge case and (b), (d) and (f) are the $--$ charge case. The arrows indicate the selected range.

categories, are given in Table I.

C. Δz Determination

The z-coordinate of each B meson decay vertex is the production point of the daughter lepton, which is determined from the intersection of the lepton track with the run-

TABLE I: Number of dilepton events

combination	on-resonance		off-resonance		continuum	
	positive	negative	positive	negative	positive	negative
ee	9059± 95.2	9028± 95.0	11± 3.3	11± 3.3	96.2± 28.9	96.2± 28.9
$\mu\mu$	14672±121.1	14014±118.4	144±12.0	100±10.0	1259.2±104.9	874.4± 87.4
$e\mu$	22802±151.0	22453±149.8	100±10.0	69± 8.3	874.4± 87.4	603.4± 72.6
total	46533±215.7	45477±213.3	255±16.0	180±13.4	2229.8±139.6	1574.0±117.3

dependent profile of the interaction point. $|\Delta z| = |z(\ell_1) - z(\ell_2)|$ is the distance between the z-coordinates of the two leptons.

In order to estimate the detector resolution in the Δz determination J/ψ decays to e^+e^- and $\mu^+\mu^-$ are used. In these events the two tracks originate from the same point, so the measured Δz, after the background contribution is subtracted, yields the detector resolution. Candidate J/ψ are selected using the same requirements as the dilepton events except the J/ψ veto. The J/ψ signal regions are defined as 3.0 GeV/c^2 < $M(e^+e^-)$ < 3.14 GeV/c^2 and 3.05 GeV/c^2 < $M(\mu^+\mu^-)$ < 3.14 GeV/c^2 and the sideband region as 3.18 GeV/c^2 < $M(\ell^+\ell^-)$ < 3.50 GeV/c^2 for both electrons and muons.

The invariant mass distributions of J/ψ candidates are fitted to a function given by

$$N(M) = h_0 e^{-\frac{(M-M_0)^2}{2S^2}} + h_1 e^{-\frac{(M-M_0)^2}{2\sigma_1{}^2}} + A(M - B)^2 + C. \qquad (4)$$

Here h_0 and h_1 are the heights of both Gaussians, M_0 is the Gaussian mean which is common to two Gaussians, σ_0 and σ_1 are the width of the Gaussians. A parameter S, given as $S = \sigma_0$ for $M \geq M_0$ and $S = \sigma_0 + \alpha(M - M_0)$ for $M < M_0$, is introduced to modify the lower mass tail of one of the Gaussians for the effect of bremsstrahlung using another parameter α. A, B and C are the parameters of the background function. The Δz distribution of the sideband region is scaled to the background yield in the signal region and subtracted from the signal region Δz distribution.

The J/ψ mass distributions and the Δz distributions are shown in Fig. 5. The RMS of the Δz distributions are 193 μm for $J/\psi \to e^+e^-$, 177 μm for $J/\psi \to \mu^+\mu^-$, and 185 μm for the combined $J/\psi \to \ell^+\ell^-$.

D. Subtraction of Continuum Events

A sample of dilepton events originating from $B\bar{B}$ events is obtained by subtracting the luminosity and cross-section scaled off-resonance data from the on-resonance data. Since the kinematics of dilepton candidates are generally different in these two data samples, the subtraction should, in principle be performed in a six dimensional (p_1^*, p_2^*, θ_1^*, θ_2^*, $\theta_{\ell\ell}^*$, Δz) space for each lepton flavour and charge combination, where $\theta_{1(2)}^*$ is the polar angle with respect to the beam axis of more(less) energetic lepton in c.m. frame. The number of $B\bar{B}$ events is obtained from

$$N_{B\bar{B}}(p_1^*, p_2^*, \theta_1^*, \theta_2^*, \theta_{\ell\ell}^*, \Delta z) = N_{\text{on}}(p_1^*, p_2^*, \theta_1^*, \theta_2^*, \theta_{\ell\ell}^*, \Delta z) - \frac{\int \mathcal{L}_{\text{on}} dt}{\int \mathcal{L}_{\text{off}} dt} \frac{s_{\text{off}}}{s_{\text{on}}} N_{\text{off}}(p_1^*, p_2^*, \theta_1^*, \theta_2^*, \theta_{\ell\ell}^*, \Delta z)$$
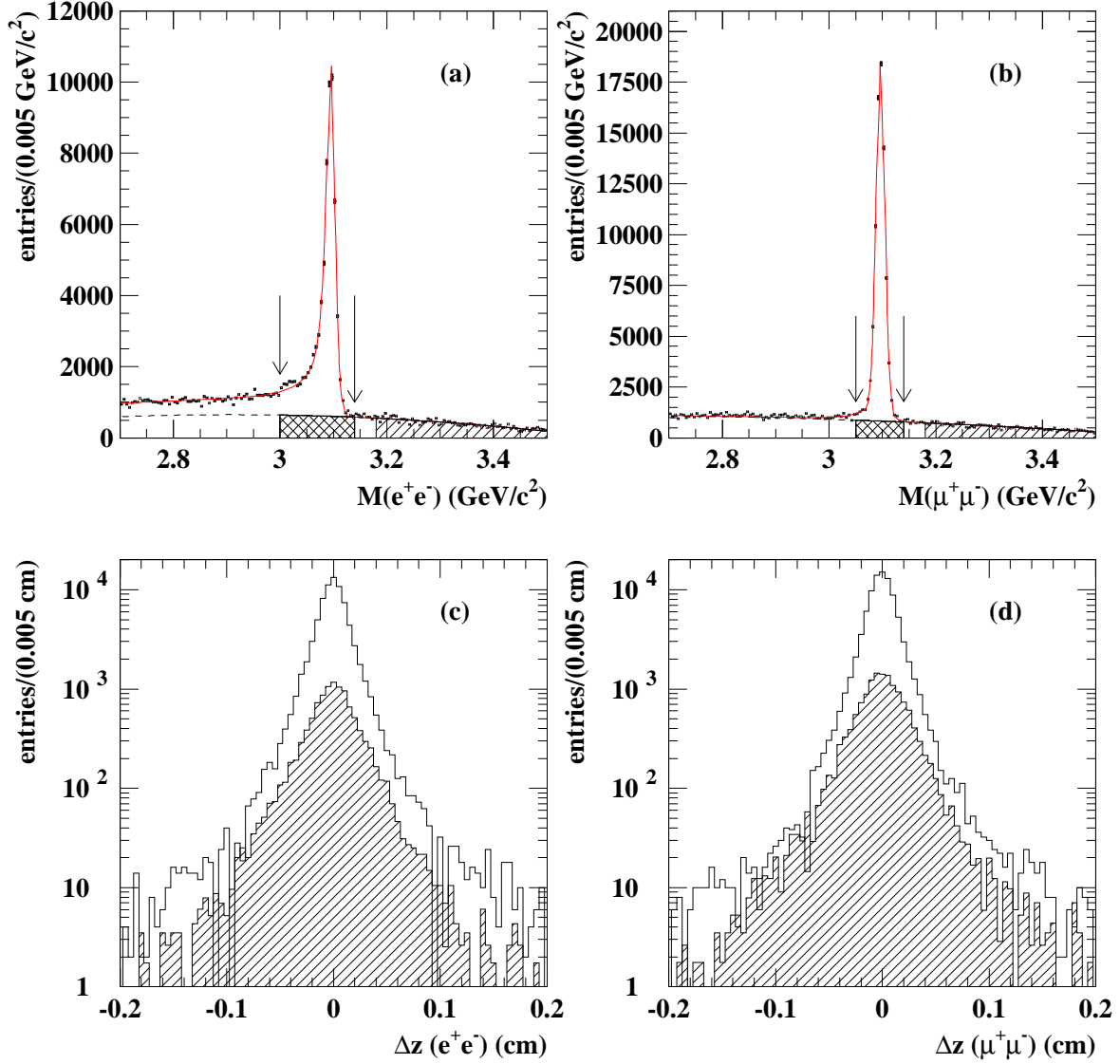
$$(5)$$

FIG. 5: Mass distributions for $J/\psi \to e^+e^-$ (a) and $J/\psi \to \mu^+\mu^-$ (b). The arrows indicate the signal region for each decay mode. The dashed lines indicate the fitted background component and the solid lines show the total fit results. The cross hatched area shows the estimated combinatorial background in the signal region and single hatched area is the sideband region used to estimate background Δz distribution. The Δz distributions for $J/\psi \to e^+e^-$ (c) and $J/\psi \to \mu^+\mu^-$ (d). Open histograms are for all J/ψ candidates in the signal region and hatched histograms are for the background.

where $N_{B\bar{B}}$ and $N_{\text{on(off)}}$ are the dilepton yields of $B\bar{B}$ origin and on(off)-resonance data, respectively, $\int \mathcal{L}_{\text{on(off)}} dt$ and $s_{\text{on(off)}}$ are the integrated luminosities and the square of c.m. energies for on(off)-resonance, respectively. $\theta^*_{\ell\ell}$ is included here because this variable behaves

distinctly differently in the two data samples for the cases containing muons, as shown in Fig. 4.

Given the available statistics, this approach is not possible. Instead, we perform the subtraction by weighting the on-resonance and off-resonance yields for one of the six kinematical variables, while integrating over the five other variables. We obtain weighting factors for the six variables by repeating this procedure. Since, t oa first approximation, the six variables are not correlated with each other, this approach provides the $B\bar{B}$ yield in the six variable space. The weighting factors are given by $w(k) = (1/r_{BB})(N_{\mathrm{on}}(k) - fN_{\mathrm{off}}(k))/N_{\mathrm{on}}(k)$ where k denotes each of six variables, f is the scaling factor for the luminosity and c.m. energy introduced in Eq. 5, and $r_{BB} \equiv N_{B\bar{B}}^{\mathrm{total}}/N_{\mathrm{on}}^{\mathrm{total}}$ is the fraction of total $B\bar{B}$ in the on-resonance yield after integrtating over all six variables and is used for the normalization. While the weighting factors show very little dependence on p_1^*, p_2^*, θ_1^*, and θ_2^* for all combinations of lepton flavours and charges, a clear dependence is observed for $\theta_{\ell\ell}^*$ in the case of $\mu\mu$ and $e\mu$ data samples as shown in Fig. 6. A clear dependence on ΔZ is also seen for all lepton pair combinations.

Using this method, the dilepton candidate yield for each lepton flavour and charge combination is then given in terms of the on-resonance yield and the weighting factors by

$$N_{B\bar{B}}(p_1^*, p_2^*, \theta_1^*, \theta_2^*, \theta_{\ell\ell}^*, \Delta z) = r_{BB} \prod_k w(k) N_{\mathrm{on}}(p_1^*, p_2^*, \theta_1^*, \theta_2^*, \theta_{\ell\ell}^*, \Delta z). \quad (6)$$

The Δz dependence of the dilepton yields are obtained by projecting $N_{B\bar{B}}(p_1^*, p_2^*, \theta_1^*, \theta_2^*, \theta_{\ell\ell}^*, \Delta z)$ onto the $|\Delta z|$ axis.

IV. RESULT

A. Corrections to lepton candidates

The number of detected leptons for each lepton flavour and charge $N_{\mathrm{det}}^{\pm}$ is related to the number of true leptons $N_{\ell}^{\pm}$ by

$$N_{\mathrm{det}}^{\pm}(p^*, \theta_{\mathrm{lab}}) = N_{\ell}^{\pm}(p^*, \theta_{\mathrm{lab}}) \varepsilon_{\mathrm{trk}}^{\pm}(p^*, \theta_{\mathrm{lab}}) \{\varepsilon_{\mathrm{pid}}^{\pm}(p^*, \theta_{\mathrm{lab}}) + \sum_{h=\pi,K,p} r_{h\ell}^{\pm}(p^*, \theta_{\mathrm{lab}}) \eta_{h\ell}^{\pm}(p^*, \theta_{\mathrm{lab}})\}, \quad (7)$$

where $\varepsilon_{\mathrm{trk}}^{\pm}$ and $\varepsilon_{\mathrm{pid}}^{\pm}$ are the efficiencies for track finding and lepton identification, $r_{h\ell}^{\pm}$ is the relative multiplicity of hadron h with respect to lepton ℓ in the $B\bar{B}$ event, and $\eta_{h\ell}^{\pm}$ is the rate of hadrons h faking leptons ℓ. The relative multiplicities are determined from $B^0\bar{B}^0$ Monte Carlo (MC) events, and are shown in Fig. 7.

Using the measured efficiencies and fake rates and the MC determined relative multiplicities, the correction factors $N_{\ell}/N_{\mathrm{det}}$ were determined in 7 bins of $p^*/\mathrm{GeV}/c$ (1.2–1.3, 1.3–1.4, 1.4–1.5, 1.5–1.6, 1.6–1.8, 1.8–2.0 and 2.0–2.3), and 8 bins of θ_{lab} (30°–37°, 37°–50°, 50°–77°, 77°–82°, 82°–111°, 111°–119°, 119°–128° and 128°–135°). The fake rates are measured in the laboratory frame. For the correction, they are converted into quantities in $(p^*, \theta_{\mathrm{lab}})$.

After the correction, the dilepton sample contains true leptons that come either from prompt neutral B meson decay (signal) or from background processes such as charged B meson decay, secondary charm decay, or other leptonic B meson processes.
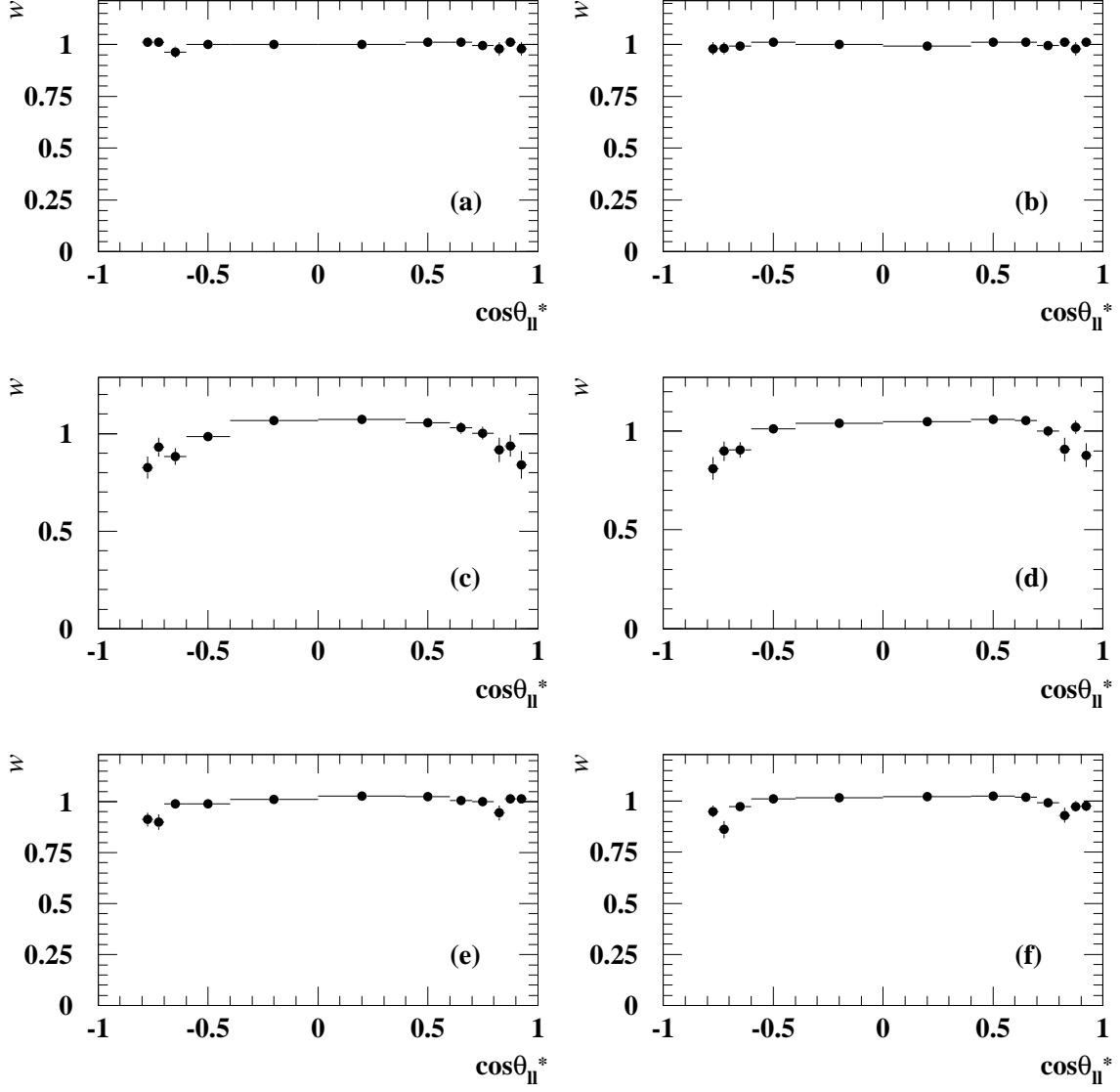
FIG. 6: $\cos\theta^*_{\ell\ell}$ dependence of the weighting factor for the fraction of the dilepton yield of $B\bar{B}$ origin in the on-resonance data for e^+e^+ (a) and e^-e^- (b) and corresponding for $\mu\mu$ (c) and (d) and $e\mu$ (e) and (f).

B. Fit to Δz Distribution

A binned maximum likelihood fit with signal and background contributions is used to extract $A_{sl}(|\Delta z|)$ from the Δz distribution. The Δz distribution for the signal events is given by Eq. 2 assuming $\Delta\Gamma$ is negligible [9] as,

$$P^{\mathrm{SS}} \propto e^{-|\Delta t|/\tau_{B^0}}(1 - \cos(\Delta m_d \Delta t)), \tag{8}$$
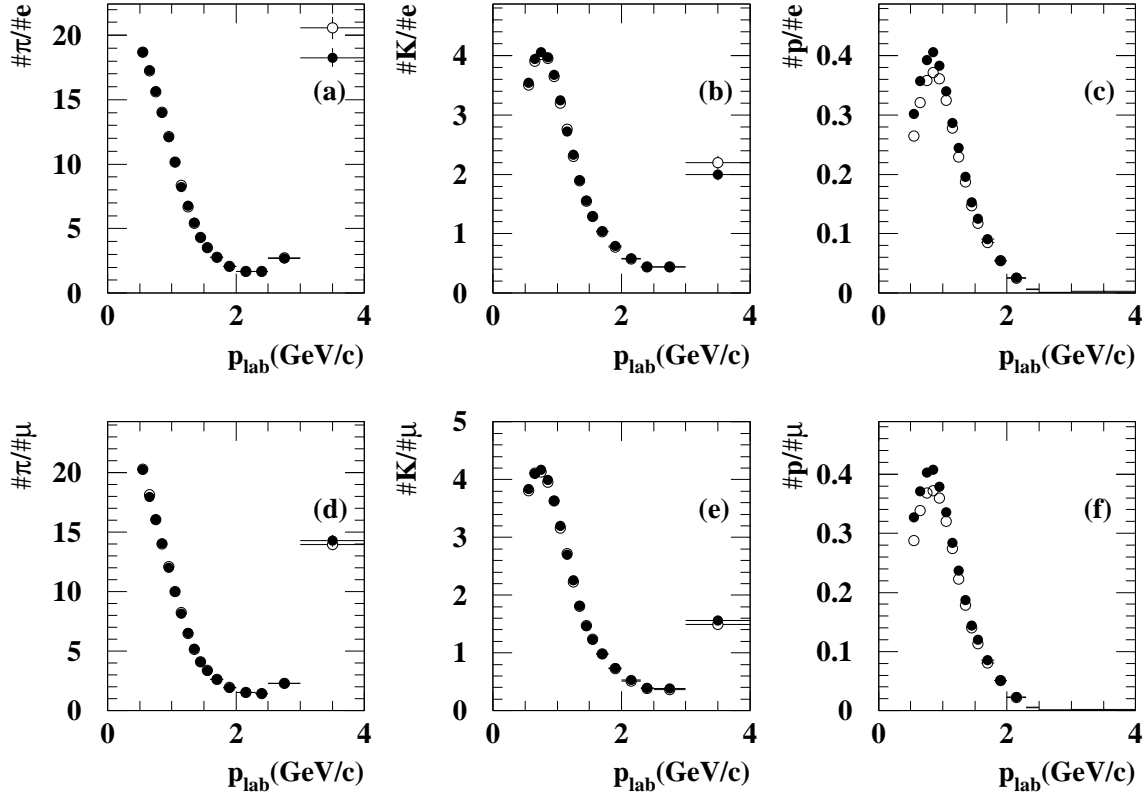
FIG. 7: Relative multiplicities of hadrons as a function of p_{lab} with respect to leptons. The hadron and lepton species are indicated on the vertical axis of each graph. Filled circles are for positive tracks and open circles are for negative tracks. Though in (a), (b), (d) and (e), the difference between positive and negative is less than 1%, in both (c) and (f), proton rate is larger than anti-proton rate by about 8%.

convolved with the detector response function described earlier. Here τ_{B^0} is the B^0 lifetime and Δm_d is the mixing parameter. These parameters are fixed to their world average values [9].

The backgrounds are placed into two categories; correctly tagged (CT), and wrongly tagged (WT). The CT category mainly contains events in which both leptons come from secondary charm decay in $\bar{B}^0 B^0 \rightarrow B^0 B^0 (\bar{B}^0 \bar{B}^0)$ (mixed) processes. The WT category contains events in which one lepton is from secondary charm decay of unmixed $B^0 \bar{B}^0$ or $B^+ B^-$ and the other is from a semi-leptonic B decay. Though background Δz distributions are estimated using MC simulations, this MC background Δz distribution overestimates the Δz resolution in the data. To correct for this the MC Δz distribution is convolved with a $\sigma = (68 \pm 19)$ μm Gaussian [10]. The Δz distributions for the true same-sign dilepton events where positive($++$) and negative($--$) samples are combined, are shown in Fig. 8 together with the fit results. The $\chi^2/n.d.f.$ of the fit is 72.17/38. In the fit, the ratio of CT to WT is fixed at the MC value, and only the ratio of signal and background is allowed to float. The

MC estimated CT and WT contributions to the Δz distribution are shown in Fig. 8.
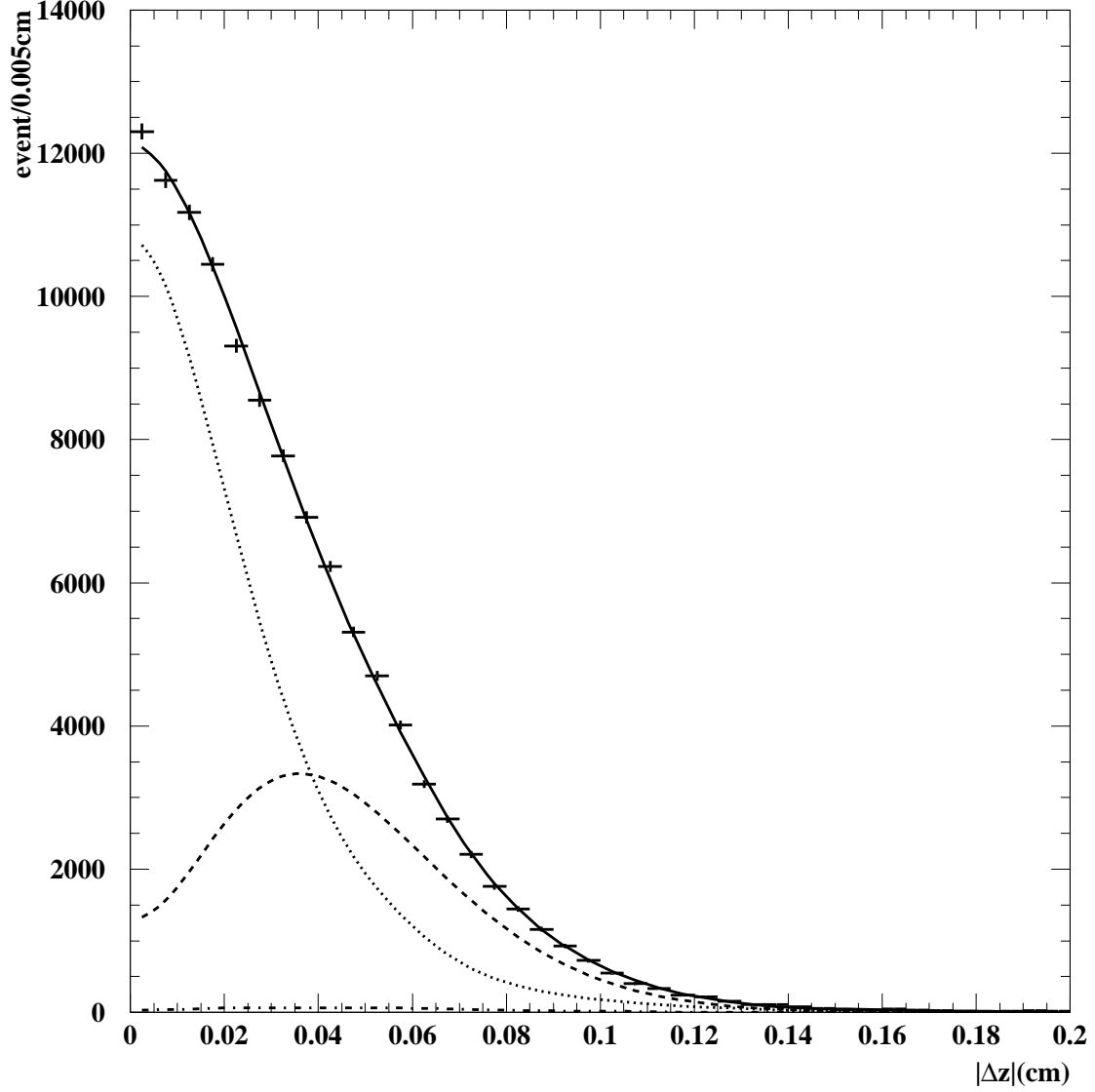

FIG. 8: Δz distribution for the true dilepton events($++$ and $--$ are combined). Points with error bars are data. The dot-dashed line shows the contribution from CT backgrounds, the dotted line shows the WT background contributions, the dashed line indicates the signal component and the solid line indicates the total of the fit.

C. Charge Asymmetry

The measured same-sign dilepton charge asymmetry is defined as

$$A_{\ell\ell}(\Delta z) = \frac{N^{++}(\Delta z) - N^{--}(\Delta z)}{N^{++}(\Delta z) + N^{--}(\Delta z)}, \tag{9}$$

where $N^{\pm\pm}(\Delta z)$ are the Δz distributions of the true dilepton yields.

Since $N^{\pm\pm}(\Delta z)$ are the sum of signal and background, $N^{\pm\pm}(\Delta z) = N_s^{\pm\pm}(\Delta z) + N_b^{\pm\pm}(\Delta z)$, the dilepton charge asymmetry A_{sl} is related to $A_{\ell\ell}$ by

$$A_{\ell\ell}(\Delta z) = \frac{N_s^{++}(\Delta z) - N_s^{--}(\Delta z)}{N_s(\Delta z)} \frac{N_s(\Delta z)}{(N_s(\Delta z) + N_b(\Delta z))} = A_{sl}(\Delta z)d(\Delta z) \tag{10}$$

where $N_s = N_s^{++} + N_s^{--}$ and $N_b = N_b^{++} + N_b^{--}$. A dilution factor, $d(\Delta z) = N_s(\Delta z)/(N_s(\Delta z) + N_b(\Delta z))$, is calculated using the signal and background yields, which are determined in the fit given in Fig. 8. The result of $A_{sl}(\Delta z)$ which is determined from measured $A_{\ell\ell}(\Delta z)$ and dilution factor $d(\Delta z)$ is shown in Fig. 9.

The dilepton charge asymmetry is $A_{sl}(|\Delta z|)$ is a time integrated quantity and does not depend on Δz. Fitting this distribution to a constant in the region of 0.015 cm $< |\Delta z| <$ 0.200 cm, yields $A_{sl} = (-0.13 \pm 0.60)\%$ and the $\chi^2/n.d.f.$ is 68.73/36. The optimum fitting range is determined using a MC study.

D. Cross Checks

As a consistency check, A_{sl} is obtained for the ee, $\mu\mu$, and $e\mu$ data samples, separately. The results, $A_{sl}(ee) = (-1.41 \pm 1.13)\%$, $A_{sl}(\mu\mu) = (+1.66 \pm 1.30)\%$, and $A_{sl}(e\mu) = (-0.44 \pm 0.94)\%$, are consistent with the primary result. Here the errors are statistical only.

In the extraction of A_{sl} from $A_{\ell\ell}(\Delta z)$ using Eq. 10, it is assumed that $N_b^{++} = N_b^{--}$. The validity of this assumption is confirmed by repeating the fit without it. This yields $N_b^{++} = 20452 \pm 126$ and $N_b^{--} = 20028 \pm 124$ in the range 0.015 cm $< |\Delta z| <$ 0.200 cm, which is consistent with the initial assumption.

E. Systematic errors

Systematic errors in the determination of A_{sl} come from uncertainties in: i) the event selection criteria, ii) corrections for efficiencies of track finding and lepton identification and for lepton misidentification, iii) the continuum subtraction, iv) the Δz fit for the dilepton sample, v) the Δz fit for the determination of A_{sl}.

Uncertainties in the event selection are estimated by repeating the analysis with varied cut values. For the track selection, the θ_{lab} cut is varied from the nominal 30°–135° to 51°–117° (barrel detector part only) in several steps, the closest-approach cut in $r\phi$ from its nominal value of 0.05 cm to 0.02 cm in six steps, the closest-approach cut in z from 2 cm to 1 cm in five steps, the p^* cut from its nominal value of 1.2 GeV/c to 1.3 GeV/c in four steps, the $\cos\theta_{\ell\ell}^*$ cut from nominal $-0.80 < \cos\theta_{\ell\ell}^* < 0.95$ to $-0.70 < \cos\theta_{\ell\ell}^* < 0.90$ in several steps, the requirement on the number of SVD hits by ± 1 from nominal value of greater or equal to two for z and one for $r\phi$. In addition, the mass cuts that reject J/ψ and $\gamma \to e^+e^-$ are widened by 20% and 50%.
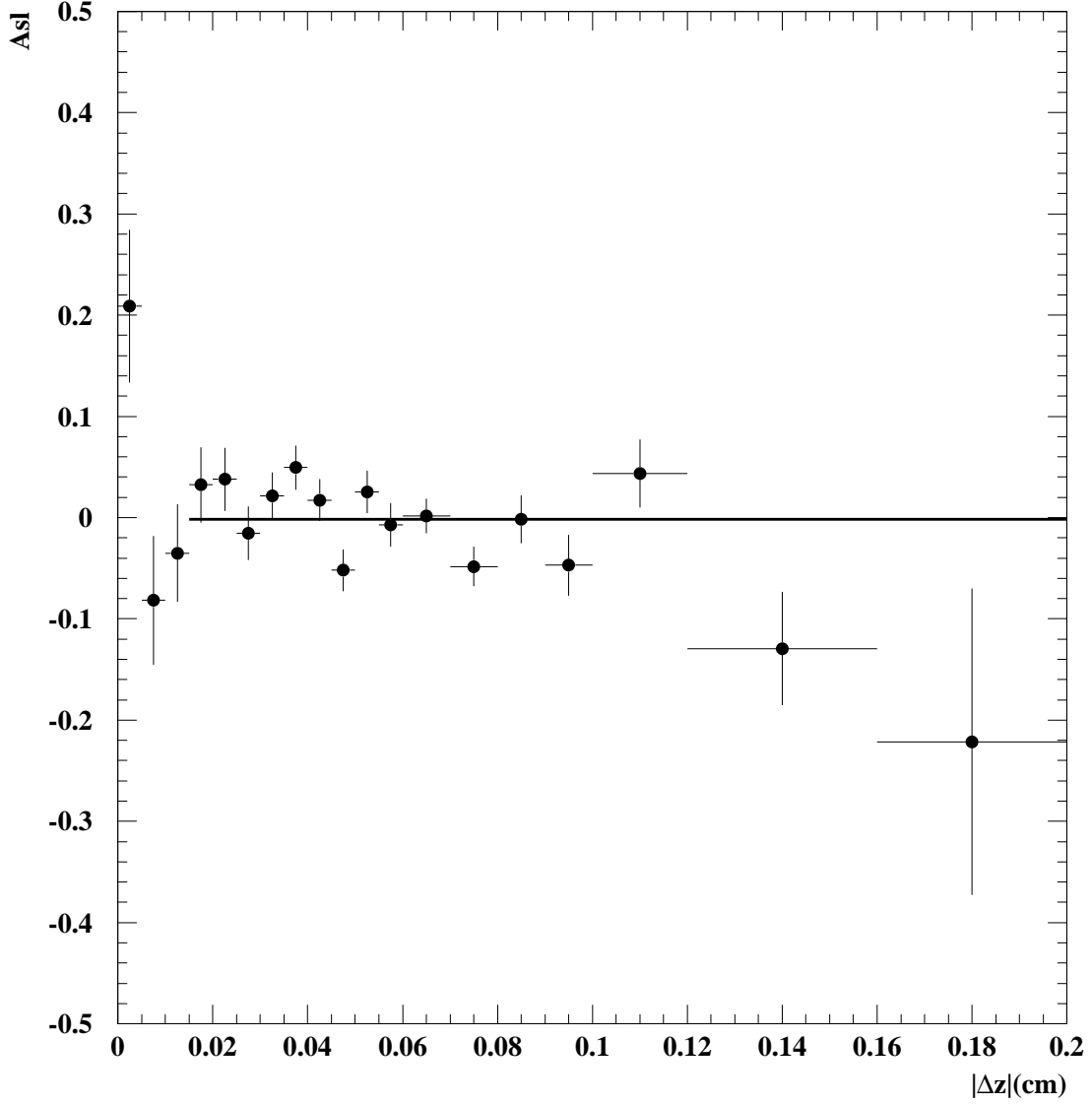
FIG. 9: $|\Delta z|$ distribution for A_{sl}.

To estimate the systematic error from the continuum subtraction, the analysis is repeated with the continuum subtraction varied by the statistical error of the off-resonance yield.

The contributions from track corrections are estimated by varying each of the efficiencies, fake rates, and relative multiplicities by $\pm 1\sigma$.

The contribution from the detector Δz response function is estimated by changing the response function width according to the statistics of Δz distribution of $J/\psi \to \ell^+\ell^-$ sample.

The contribution from the 68 μm smearing is estimated by repeating the analysis with 50 μm and 87 μm smearing, which are the values obtained when the χ^2 for the Δz fit is changed by one compared with the default fit. The contributions from uncertainties in Δm_d

and τ_{B^0} are also estimated by varying the nominal values by $\pm 1\sigma$. The dilution factor fitting range is varied from nominal 0.00 cm $< |\Delta z| <$ 0.20 cm to 0.00 cm $< |\Delta z| <$ 0.05 cm.

For the fitting range for the determination of the final A_{sl}, the lower limit is varied from its nominal value of 0.015 cm to 0.040 cm in several steps.

The results of the systematic error determination for A_{sl} are summarized in Table II.

TABLE II: Source of systematic errors for the measurement of A_{sl}

category	source	ΔA_{sl} (%)
event selection	track selection	± 0.236
	$\cos\theta^*_{\ell\ell}$ cut	± 0.107
	lepton pair veto	± 0.167
continuum subtraction		± 0.314
track corrections	track finding efficiency	± 0.074
	electron identification efficiency	± 0.058
	muon identification efficiency	± 0.208
	fake electrons	± 0.031
	fake muons	± 0.047
	relative multiplicity	± 0.057
Δz fit for dileptons	detector response function	± 0.009
	Δm_d	± 0.011
	τ_{B^0}	± 0.009
	68 μm smearing of background Δz	± 0.009
	statistics of background MC	± 0.022
	fitting range	± 0.004
	assuming $N_b^{++} = N_b^{--}$	± 0.139
Δz fit for A_{sl}	fitting range	± 0.207
total		± 0.561

V. CONCLUSION

The charge asymmetry for same-sign dilepton events $\Upsilon(4S)$ decays has been measured. The result is related to a CP-violation parameter in B^0-$\bar{B}^0$ mixing, $A_{sl} = (-0.13 \pm 0.60(\text{stat}) \pm 0.56(\text{sys}))\%$, or equivalently $|q/p| = 1.0006 \pm 0.0030(\text{stat}) \pm 0.0028(\text{sys})$. The measured A_{sl} is consistent with zero, or equivalently, $|q/p|$ is consistent with unity. This implies CP-violation in B^0-$\bar{B}^0$ mixing is below the $O(10^{-2})$ level. The CP-violation parameter ϵ_B can be calculated as $Re(\epsilon_B)/(1 + |\epsilon_B|^2) = (-0.3 \pm 1.5(\text{stat}) \pm 1.4(\text{sys})) \times 10^{-3}$, using the exact formula

$$\frac{Re(\epsilon_B)}{1 + |\epsilon_B|^2} = 0.5 \frac{1 - \sqrt{(1 - A_{sl})/(1 + A_{sl})}}{1 + \sqrt{(1 - A_{sl})/(1 + A_{sl})}}. \tag{11}$$

These results are consistent with and provide significantly more restrictive bounds than previous measurements [11].

19

Acknowledgments

[1] A.B. Carter and A.I. Sanda, Phys. Rev. Lett. **45**, 952 (1980); Phys. Rev. **D23**, 1567 (1981).

[2] See, for example, A. Mohapatra, M. Satpathy, K. Abe, and Y. Sakai, Phys. Rev. D 58, 036003 (1998), and references therein.

[3] R. N. Cahn and M. P. Worah, Phys. Rev. **D60**, 76006 (1999), Y. Nir, 27th SLAC Summer Institute on Particle Physics (1999), hep-ph/9911321, and references therein.

[4] Belle Collaboration, A. Abashian *et al.* , Nucl. Instr. and Meth. **A479**, 117 (2002).

[5] K. Akai *et al.* , Nucl. Instr. And Meth. **A499**, 191 (2003)

[6] K. Hanagaki *et al.*, Nucl. Instr. and Meth. **A485**, 490 (2002).

[7] A. Abashian *et al.*, Nucl. Instr. and Meth. **A491**, 69 (2002).

[8] G. Fox and S. Wolfram, Phys. Rev. Lett. **41**, 1581 (1978).

[9] Particle Data Group, S. Eidelman et al., Phys. Lett. B **592**, 1 (2004)

[10] Belle Collaboration, N. Hastings *et al.*, Phys. Rev. **D67** 052004 (2003).

[11] CDF Collaboration, F. Abe *et al.*, Phys. Rev. **D55**, 2546 (1996); OPAL Collaboration, G. Abbiendi *et al.*, Eur. Phys. J. **C12**, 609 (2000); ALEPH Collaboration, R. Barate *et al.*, Eur. Phys. J. **C20**, 431 (2001); CLEO Collaboration, D.E. Jaffe *et al.*, Phys. Rev. Lett. **86**, 5000 (2001); BABAR Collaboration, B. Aubert *et al.*, Phys. Rev. Lett. **88**, 231801 (2002);